PERGAMON

International Journal of Heat and Mass Transfer 44 (2001) 4127–4138

International Journal of HEAT and MASS TRANSFER

www.elsevier.com/locate/ijhmt

The onset of convection in an inclined anisotropic porous layer

D.A.S. Rees [a,*], A. Postelnicu [b]

[a] Department of Mechanical Engineering, University of Bath, Claverton Down, Bath BA2 7AY, UK

[b] Department of Thermo and Fluid Mechanics, Transylvania University of Brasov, Bdul. Eroilor No. 29, Brasov 2200, Romania

Received 18 September 2000

Abstract

We consider the onset of convection in a porous layer heated from below. The layer is anisotropic with respect to both its permeability and diffusivity and is inclined to the horizontal. The aim of this work is to determine not only by how much the critical Rayleigh number varies when the layer is inclined, but also the wave number and the angle the roll makes with the direction about which the layer is inclined. We find that there is not always an abrupt transition between longitudinal and transverse rolls as the governing parameters are varied, but there is often a smooth transition between these states.

Keywords: Free convection; Porous layer; Anisotropy; Onset

1. Introduction

One of the most widely studied and fundamental processes in the study of convection in fluid-saturated porous media is the onset and development of convection in layers heated from below. The pioneering works in the field were carried out by Horton and Rogers [1] and Lapwood [2], and the general problem has become known as the Horton–Rogers–Lapwood or Darcy–Bénard problem. A fairly comprehensive account of the current state-of-the-art may be found in Rees [3]. In its classical formulation a porous medium is sandwiched between two uniform temperature plane surfaces and is heated from below.

While there are many different extensions to Darcy's law, we focus solely on the effects of introducing anisotropy where the principal axes of the permeability and diffusivity tensors coincide with the coordinate directions. The first work to deal with such problems was undertaken by Castinel and Combarnous [4], and detailed reviews of anisotropic convection may be found in Storesletten [5] and Vasseur and Robillard [6].

In this paper, we investigate in detail how the inclination of the layer away from the horizontal affects the criterion for the onset of anisotropic convection. It is well-known from theoretical investigations that longitudinal vortices with axes directly up the layer are favoured when the layer is isotropic; see Rees and Bassom [7], for example, who give a very detailed analysis of tilted isotropic layers.

Apart from the companion paper [8], only Storesletten and Tveitereid [9] deals with the combined effects of anisotropy and layer inclination. The authors of [9] assumed that the preferred mode of convection at onset takes the form of either a longitudinal vortex (where the vortex is aligned parallel to the mean flow direction), or a transverse roll (which is perpendicular to the longitudinal roll). In that paper conditions are given in which transverse modes are preferred to longitudinal vortices at relatively low but nevertheless O(1) inclinations.

One of the aims of this paper and of its predecessor [8] is to determine whether the sharp transition assumption found in [9] is valid. The results contained in [8], which considers small inclinations from the horizontal, show that Storesletten and Tveitereid were correct in assuming a sudden transition but we show here that this assumption is, in fact, invalid for O(1) inclinations. We find that there are parameter regimes where there is a smooth transition, in terms of the preferred

* Corresponding author. Tel.: +44-1225-826775; fax: +44-1225-826928.

E-mail address: ensdasr@bath.ac.uk (D.A.S. Rees).

0017-9310/01/$ - see front matter
PII: S0017-9310(01)00055-2

Nomenclature

$\underline{\underline{D}}$	diffusivity tensor
f, g, q, F, G, Q	small perturbations
$\underline{g}$	gravity vector
h	height of layer
$\underline{i}, \underline{j}, \underline{k}$	unit vectors in the x, y and z directions, respectively
k	wave number
$\underline{\underline{K}}$	permeability tensor
p	pressure
R	Darcy–Rayleigh number
t	time
T_c	temperature of cooled surface
T_h	temperature of heated surface
T	temperature
T_m	mean temperature
u	fluid flux velocity in the x direction
v	fluid flux velocity in the y direction
w	fluid flux velocity in the z direction
x	Cartesian coordinate up the inclined layer
y	Cartesian coordinate across the layer
z	horizontal Cartesian coordinate across the layer
Greek symbols	
μ	viscosity
ρ_0	reference density
β	coefficient of cubical expansion
σ	heat capacity ratio
ξ	modified permeability ratios
ξ_1, ξ_3	permeability ratios
η	modified diffusivity ratios
η_1, η_3	diffusivity ratios
α	layer inclination
ψ, Ψ	streamfunction
ϕ	orientation of roll
θ, Θ	scaled temperature
λ	complex exponential growth rate
Superscripts and subscripts	
$'$	differentiation with respect to y
i	imaginary part
1, 2, 3	x, y and z components of the permeability and diffusivity tensors, respectively

roll orientation, between the transverse and the longitudinal roll as the angle of inclination increases. There are also regimes where the transition is smooth until a particular oblique orientation is achieved, and then there is a sudden change to the longitudinal roll. The fundamental problem we solve has five independent parameters (two diffusivity ratios, two permeability ratios and the angle of tilt) and therefore we cannot hope to give a comprehensive account of the whole of parameter space. Nevertheless, we hope that the results presented allow a good qualitative understanding of the preferred form of destabilisation of an anisotropic layer.

2. Equations of motion

We consider the onset of convection in a tilted anisotropic porous layer heated from below. The layer is of thickness h and is inclined at an angle α to the horizontal. The horizontal z-axis forms the direction about which the layer has been rotated, the y-axis is perpendicular to the bounding surfaces, and the x-axis lies in the lower surface pointing up the plane. We assume that Boussinesq approximation holds, and that no other extension to Darcy's law is present except for anisotropy in the permeability and diffusivity. Therefore, the flow and heat transfer are governed by the equations

$$\nabla \cdot \underline{u} = 0, \tag{1}$$

$$\mu \underline{u} + \underline{\underline{K}} \cdot (\nabla p + \rho_0 \beta (T - T_m) \underline{g}) = 0, \tag{2}$$

$$\sigma \frac{\partial T}{\partial t} + \underline{u} \cdot \nabla T = \nabla \cdot (\underline{\underline{D}} \cdot \nabla T), \tag{3}$$

where the permeability and diffusivity tensors have their principal axes in the coordinate directions and are given by

$$\underline{\underline{K}} = K_1 \underline{i}\underline{i} + K_2 \underline{j}\underline{j} + K_3 \underline{k}\underline{k}, \tag{4}$$

$$\underline{\underline{D}} = D_1 \underline{i}\underline{i} + D_2 \underline{j}\underline{j} + D_3 \underline{k}\underline{k}. \tag{5}$$

The vectors, $\underline{i}$, $\underline{j}$ and $\underline{k}$ are the unit vectors in the x, y and z directions, respectively. Terms in (1)–(3) have their familiar meanings in the porous medium context and these are given in the nomenclature.

We non-dimensionalise using the following substitutions:

$$(x, y, z) = h(x^*, y^*, z^*), \quad \underline{u} = D_2 h \underline{u}^*, \quad t = \frac{\sigma h^2}{D_2} t^*, \tag{6}$$

$$p = \frac{D_2 \mu}{K_2} p^*, \quad T = T_c + (T_h - T_c)\theta, \tag{7}$$

and obtain

$$\nabla \cdot \underline{u} = 0, \tag{8}$$

$$u = -\frac{K_1}{K_2}\left(\frac{\partial p}{\partial x} + R\left(\theta - \frac{1}{2}\right)\sin\alpha\right), \tag{9}$$

$$v = -\left(\frac{\partial p}{\partial y} + R\left(\theta - \frac{1}{2}\right)\cos\alpha\right), \tag{10}$$

$$w = -\frac{K_3}{K_2}\frac{\partial p}{\partial z}, \tag{11}$$

$$\frac{\partial \theta}{\partial t} + \underline{u}\cdot\nabla\theta = \frac{D_1}{D_2}\frac{\partial^2\theta}{\partial x^2} + \frac{\partial^2\theta}{\partial y^2} + \frac{D_3}{D_2}\frac{\partial^2\theta}{\partial z^2}, \tag{12}$$

where the asterisk superscript has been omitted for clarity of presentation. As in [8] we consider both two-dimensional and three-dimensional modes of instability. For two-dimensional convection we define a stream-function, ψ, using

$$u = -\frac{\partial\psi}{\partial y}, \quad v = \frac{\partial\psi}{\partial x}, \quad w = 0, \tag{13}$$

whereas for three-dimensional convection we eliminate $\underline{u}$ to obtain a system of equations in terms of pressure and temperature only. Thus, in the former case we consider the equations

$$\xi_1\frac{\partial^2\psi}{\partial x^2} + \frac{\partial^2\psi}{\partial y^2} = R\xi_1\left(\frac{\partial\theta}{\partial x}\cos\alpha - \frac{\partial\theta}{\partial y}\sin\alpha\right), \tag{14}$$

$$\frac{\partial\theta}{\partial t} + \frac{\partial\psi}{\partial x}\frac{\partial\theta}{\partial y} - \frac{\partial\psi}{\partial y}\frac{\partial\theta}{\partial x} = \eta_1\frac{\partial^2\theta}{\partial x^2} + \frac{\partial^2\theta}{\partial y^2} \tag{15}$$

subject to

$$\psi = 0,\ \theta = 1 \ \text{ on } \ y = 0$$
$$\text{and} \quad \psi = 0,\ \theta = 0 \ \text{ on } \ y = 1 \tag{16}$$

and in the latter case we use

$$\xi_1\frac{\partial^2 p}{\partial x^2} + \frac{\partial^2 p}{\partial y^2} + \xi_3\frac{\partial^2 p}{\partial z^2} = R\left[\xi_1\frac{\partial\theta}{\partial x}\sin\alpha + \frac{\partial\theta}{\partial y}\cos\alpha\right], \tag{17}$$

$$\frac{\partial\theta}{\partial t} + R\left[\xi_1\frac{\partial\theta}{\partial x}\sin\alpha + \frac{\partial\theta}{\partial y}\cos\alpha\right]\theta - \xi_1\frac{\partial p}{\partial x}\frac{\partial\theta}{\partial x} - \frac{\partial p}{\partial y}\frac{\partial\theta}{\partial y} - \xi_3\frac{\partial p}{\partial z}\frac{\partial\theta}{\partial z} = \eta_1\frac{\partial^2\theta}{\partial x^2} + \frac{\partial^2\theta}{\partial y^2} + \eta_3\frac{\partial^2\theta}{\partial z^2} \tag{18}$$

subject to

$$\frac{\partial p}{\partial y} = \frac{1}{2}\cos\alpha,\ \theta = 1 \ \text{ on } \ y = 0$$
$$\text{and} \quad \frac{\partial p}{\partial y} = -\frac{1}{2}\cos\alpha,\ \theta = 0 \ \text{ on } \ y = 1. \tag{19}$$

The non-dimensional parameter,

$$R = \frac{\rho_0 g\beta K_2(T_h - T_c)h}{\mu D_2} \tag{20}$$

is the Darcy–Rayleigh number based upon the permeability and diffusivity in the y-direction, and

$$\xi_1 = \frac{K_1}{K_2}, \quad \xi_3 = \frac{K_3}{K_2}, \quad \eta_1 = \frac{D_1}{D_2}, \quad \eta_3 = \frac{D_3}{D_2} \tag{21}$$

are permeability and diffusivity ratios.

The linear stability characteristics are obtained by first linearising Eqs. (14) and (15), and Eqs. (17) and (18) about the basic flow profiles by means of the substitutions

$$\psi = -\frac{1}{2}R\xi_1(y - y^2)\sin\alpha + \Psi, \quad \theta = 1 - y + \Theta,$$
$$p = \frac{1}{2}R(y - y^2)\cos\alpha + P, \tag{22}$$

where the magnitudes of Ψ, Θ and P are assumed to be infinitesimally small. We therefore obtain the following linearised perturbation equations in two-dimensions:

$$\xi_1\frac{\partial^2\Psi}{\partial x^2} + \frac{\partial^2\Psi}{\partial y^2} = R\xi_1\left(\frac{\partial\Theta}{\partial x}\cos\alpha - \frac{\partial\Theta}{\partial y}\sin\alpha\right), \tag{23}$$

$$\frac{\partial\Theta}{\partial t} = \eta_1\frac{\partial^2\Theta}{\partial x^2} + \frac{\partial^2\Theta}{\partial y^2} + \frac{\partial\Psi}{\partial x} + R\xi_1\sin\alpha\left(y - \frac{1}{2}\right)\frac{\partial\Theta}{\partial x}, \tag{24}$$

and in three-dimensions,

$$\xi_1\frac{\partial^2\rho}{\partial x^2} + \frac{\partial^2\rho}{\partial y^2} + \xi_3\frac{\partial^2\rho}{\partial z^2} = R\left[\xi_1\frac{\partial\Theta}{\partial x}\sin\alpha + \frac{\partial\Theta}{\partial y}\cos\alpha\right], \tag{25}$$

$$\frac{\partial\Theta}{\partial t} = \eta_1\frac{\partial^2\Theta}{\partial x^2} + \frac{\partial^2\Theta}{\partial y^2} + \eta_3\frac{\partial^2\Theta}{\partial z^2} + R\cos\alpha\Theta + R\xi_1 \times \sin\alpha\left(y - \frac{1}{2}\right)\frac{\partial\Theta}{\partial x} - \frac{\partial P}{\partial y} \tag{26}$$

subject to

$$\Psi = \Theta = \frac{\partial P}{\partial y} = 0 \quad \text{on both } y = 0 \text{ and } y = 1. \tag{27}$$

As in [8] we Fourier-decompose the disturbances in the x and z directions which reduces the perturbation equations to ordinary differential eigenvalue form. We therefore substitute

$$\Psi = \mathrm{i}f(y)\mathrm{e}^{\mathrm{i}kx+\lambda t}, \quad \Theta = g(y)\mathrm{e}^{\mathrm{i}kx+\lambda t} \tag{28}$$

into (23) and (24) to obtain

$$f'' - k^2\xi_1 f = R\xi_1[(k\cos\alpha)g + (\mathrm{i}\sin\alpha)g'], \tag{29}$$

$$g'' - k^2\eta_1 g = kf - (Rik\xi_1\sin\alpha)\left(y - \frac{1}{2}\right)g + \lambda g \tag{30}$$

subject to $f = g = 0$ at $y = 0, 1$. Here k is the wave number of the disturbance and λ is the exponential

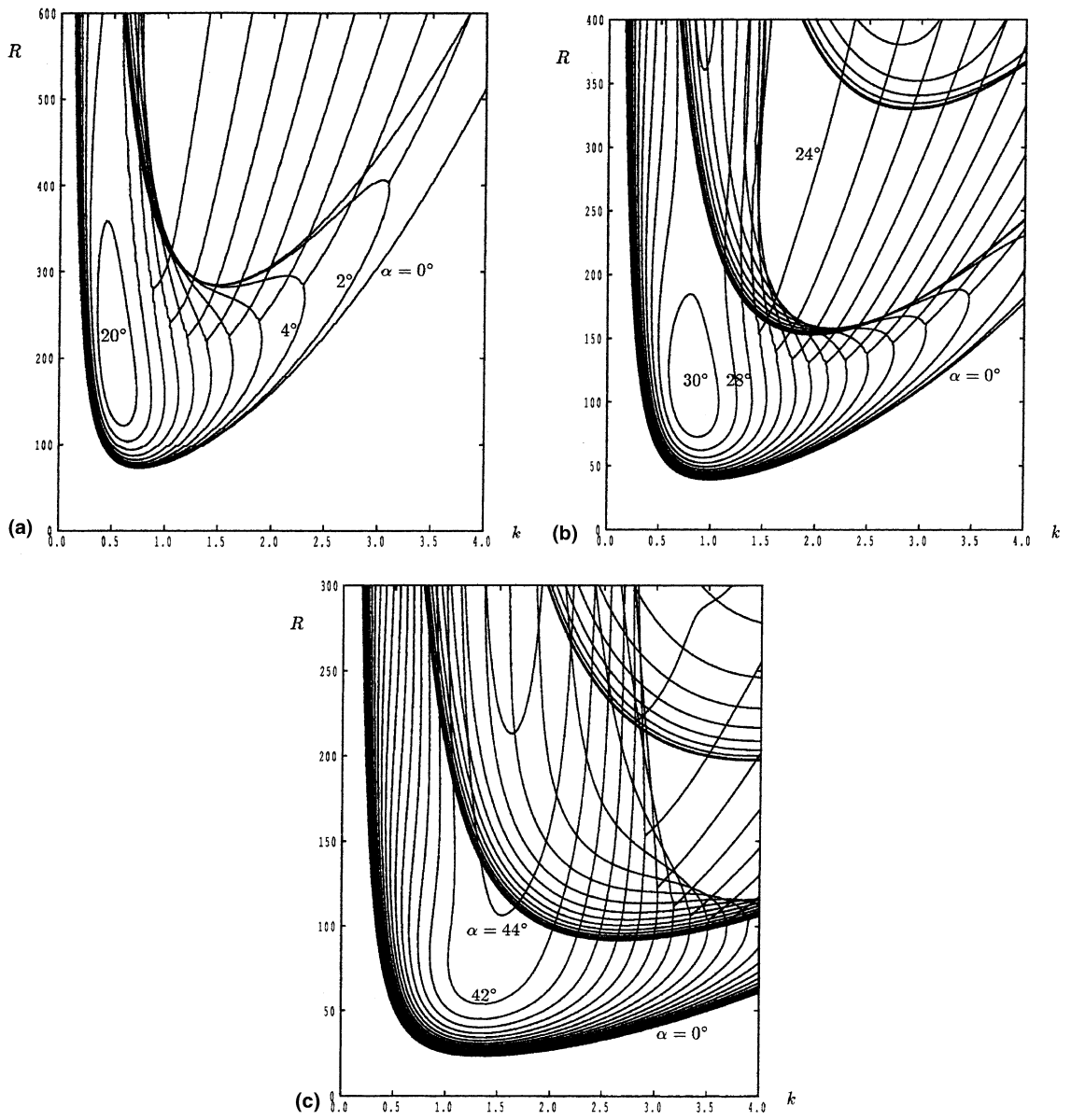

Fig. 1. Detailed neutral curves for the onset of two-dimensional convection in layers with $\eta_1 = 1$ for: (a) $\xi_1 = 3$, (b) $\xi_1 = 1$, (c) $\xi_1 = 0.3$. The lowest curve in each case corresponds to a horizontal layer ($\alpha = 0°$) and each successive curve corresponds to an increment of 2°.

growth rate. For three-dimensional disturbances we substitute

$$P = q(y)\mathrm{e}^{\mathrm{i}k(z\cos\phi + x\sin\phi)+\lambda t},$$
$$\Theta = g(y)\mathrm{e}^{\mathrm{i}k(z\cos\phi + x\sin\phi)+\lambda t} \tag{31}$$

into Eqs. (25) and (26) to obtain

$$q'' - k^2(\xi_1\sin^2\phi + \xi_3\cos^2\phi)q = R\left[(\cos\alpha)g' + (\mathrm{i}k\xi_1\sin\phi\sin\alpha)g\right], \tag{32}$$

$$g'' + \left[R\cos\alpha - k^2(\eta_1\sin^2\phi + \eta_3\cos^2\phi)\right]g = q' - (Rik\xi_1\sin\phi\sin\alpha)\left(y - \frac{1}{2}\right)g + \lambda g \tag{33}$$

subject to $q' = g = 0$ at $y = 0, 1$. Here ϕ represents the orientation of the axis of the vortex disturbance relative to the x-direction. The value $\phi = 90°$ represents the two-dimensional case and is termed a transverse roll, $\phi = 0°$ represents the longitudinal roll, and rolls of other orientations are called oblique.

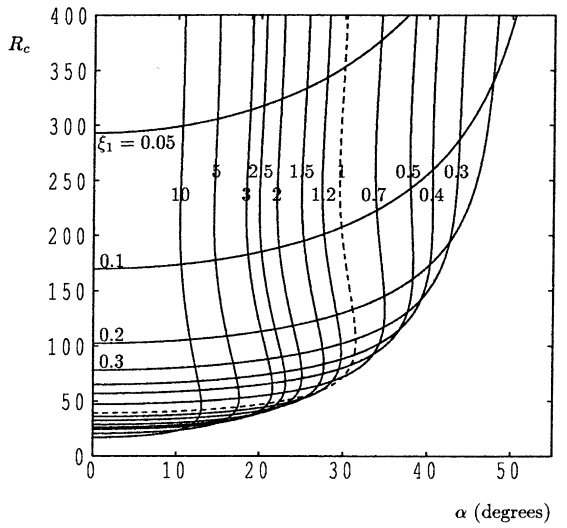

Fig. 2. Variation of the critical values of R with α for two-dimensional convection for different values of ξ_1 with $\eta_1 = 1$. The curves for $\xi_1 = 3$, 1 and 0.3 correspond to the maximum and minimum values of the neutral curves shown in Fig. 1. Anisotropy corresponds to the dashed line.

In this paper, we consider first two-dimensional disturbances, for although there exist parameter sets for which three-dimensional disturbances are more destabilising, it is always possible to eliminate three-dimensionality by restricting the layer sufficiently in the spanwise (or z) direction with impermeable insulating sidewalls.

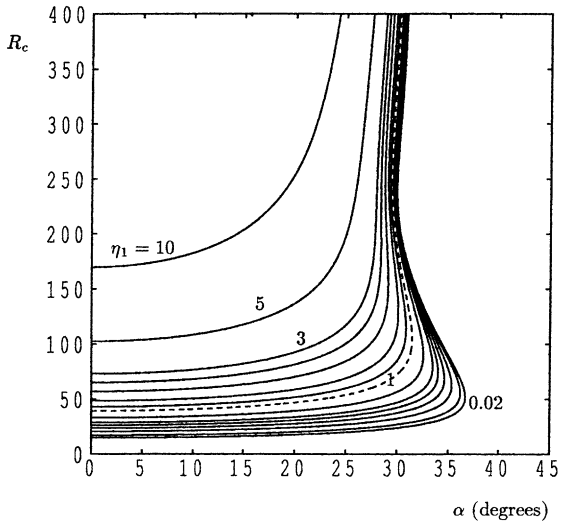

Fig. 3. Variation of the critical values of R with α for two-dimensional convection for different values of η_1 with $\xi_1 = 1$. The values of η_1 are 0.02, 0.05, 0.1, 0.2, 0.3, 0.5, 0.7, 1.0, 1.2, 1.5, 2.0, 2.5, 3.0, 5.0 and 10.0. Anisotropy corresponds to the dashed line.

3. Two-dimensional instabilities

At O(1) inclinations Eqs. (29) and (30) must be solved numerically. The method chosen to elucidate the global stability properties is identical to that used in Rees and Bassom [7] who considered the equivalent isotropic layer. The ordinary differential eigenvalue problem was transformed into a matrix eigenvalue problem by first discretising the equations using central differences on a uniform grid, then solving for the vector of f-values in terms of the g-values using the approximation to Eq. (29), and by substitution of this into the approximation of Eq. (30). The resulting complex matrix eigenvalue problem for λ was solved using the NAG library routine F02AJF. This method was applied over a range of values of R and k for distinct values of α and the neutral curves were obtained by employing a contouring routine to $Re(\lambda)$ to identify where this is equal to zero.

Typical results of this process are shown in the various subfigures of Fig. 1 which correspond to the cases $\xi_1 = 3$, $\xi_1 = 1$, $\xi_1 = 0.3$, where $\eta_1 = 1$. Isotropy corresponds to the case $\xi_1 = 1$ and it is clear in all three cases that the critical Rayleigh number increases with increasing inclination. Of most importance is the lowest point of these neutral curves where $\partial R/\partial k = 0$ and Fig. 2 shows the variation of such values of R with α. Of course this zero-slope condition also corresponds to maxima in the curves; see the top of the $\alpha = 30°$ curve in Fig. 1(b), for example. For $\xi_1 = 1$ the maximum slope for which there is instability is $\alpha = 31.49°$ and the neutral curve given in Fig. 1(b) tends towards the asymptotic value $\alpha = 31.30°$ at large values of R; see [7]. Therefore, $\alpha = 31.49°$ is the largest inclination for which two-dimensional linear instability may arise. This maximum inclination decreases as ξ_1 increases – $\alpha_{\max}$ is approximately 21° for $\xi_1 = 3.0$, and is greater than 47° for $\xi_1 = 0.3$. Once ξ_1 is less than 0.4 then the asymptotic value of α at large values of R assumes importance since the local maximum and minimum which exist at lower values of R have coalesced.

In Fig. 3, we see the equivalent behaviour for the anisotropic diffusivity cases with $\xi_1 = 1$. For a fixed inclination the critical Rayleigh number typically rises as η_1 increases. Again we see a pronounced local maximum inclination for the presence of instability for any chosen value of η_1, although this is true only for values less than roughly 3.0.

4. Three-dimensional instabilities

The analysis in [7] shows that $\phi = 0°$ forms the preferred mode for all inclinations of an isotropic layer. However, Storesletten and Tveitereid [9] showed that there are many circumstances when transverse modes

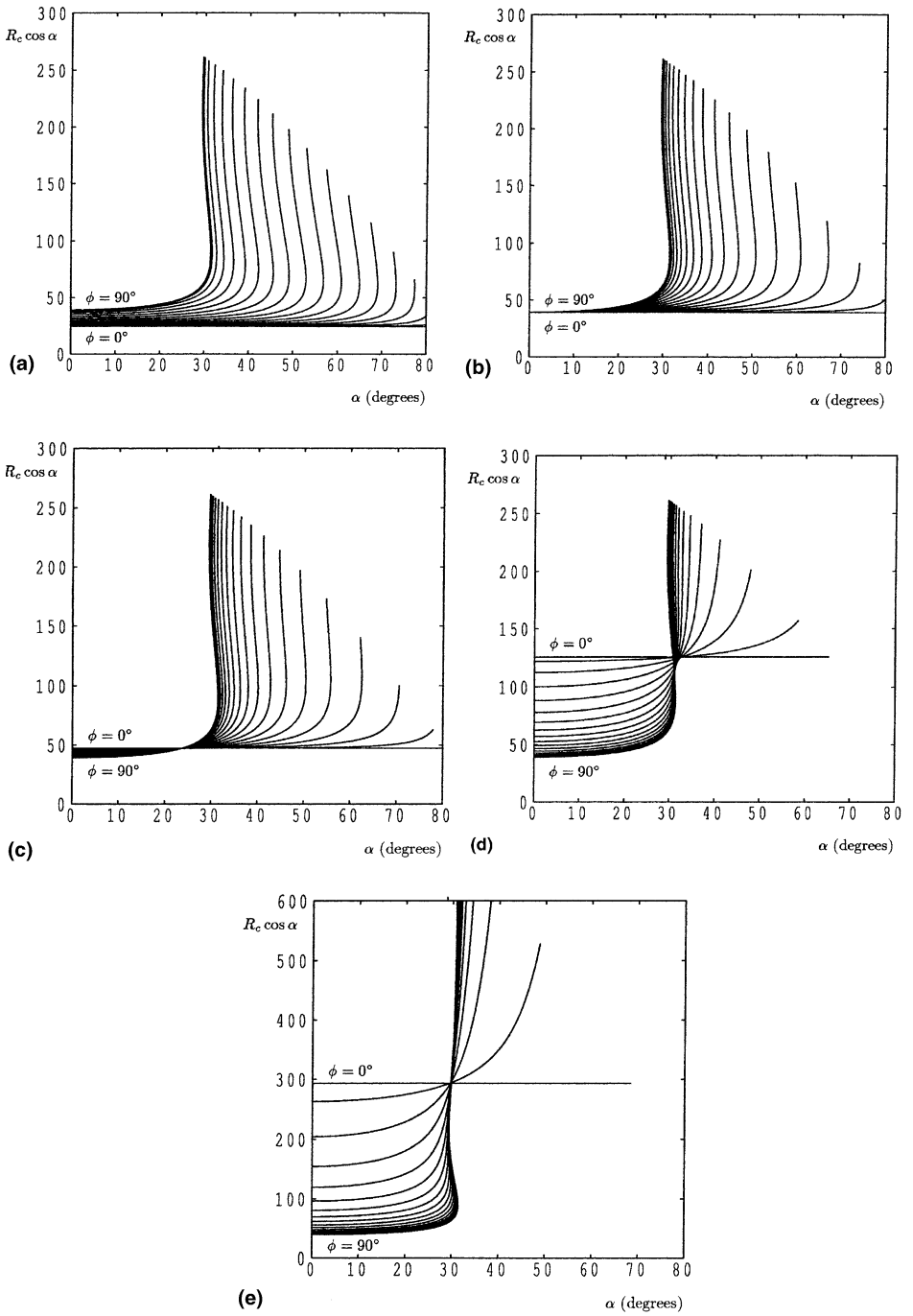

Fig. 4. Variation of R_c with α for various roll orientations from $\phi = 0°$ to $\phi = 90°$. Curves are plotted at increments of 5° in ϕ. Here we assume that the layer is thermally isotropic ($\eta_1 = \eta_3 = 1$) with $\xi_1 = 1$ and (a) $\xi_3 = 3$, (b) $\xi_3 = 1$, (c) $\xi_3 = 0.7$, (d) $\xi_3 = 0.15$, (e) $\xi_3 = 0.05$.

($\phi = 90°$) are favoured over longitudinal modes. The aim of this section is to examine in detail the behaviour of oblique modes and to determine if and when these supercede both longitudinal and transverse modes in importance. A secondary aim is to provide a good qualitative understanding of modal transitions as the non-dimensional parameters vary. Given that there are five parameters (namely, α, ξ_1, ξ_3, η_1, η_3) it would be

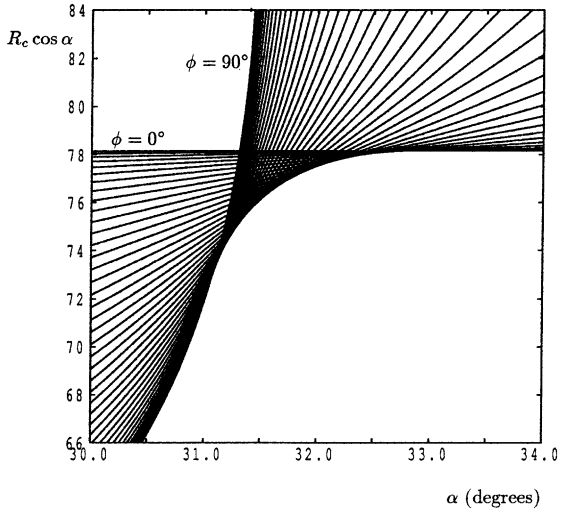

Fig. 5. A close-up view of the neutral curves for $\xi_3 = 0.3$ (with $\xi_1 = \eta_1 = \eta_3 = 1$) for roll orientations between $\phi = 0°$ and $\phi = 90°$. Curves are plotted at increments of 2° in ϕ. This figure shows the smooth transition in the preferred roll orientation as the layer inclination changes.

unreasonable to be comprehensive in presenting quantitative results. Therefore, we restrict our quantitative presentation to the thermally isotropic case for which $\eta_1 = \eta_3 = 1$.

It is only possible to make analytical progress at O(1) inclinations for longitudinal rolls. In this case the onset Rayleigh number for general values of k is

$$R = \frac{(\pi^2 + k^2\xi_3)(\pi^2 + k^2\eta_3)}{k^2\xi_3 \cos\alpha}. \tag{34}$$

The minimising wave number and the corresponding critical Rayleigh number are

$$k_c = \frac{\pi}{(\xi_3\eta_3)^{1/4}} \tag{35}$$

and

$$R_c = \pi^2\left[1 + \left(\frac{\eta_3}{\xi_3}\right)^{1/2}\right]^2 \Big/ \cos\alpha. \tag{36}$$

Here we see clearly that $R_c \to \infty$ as $\alpha \to (1/2)\pi$, the vertical limit. This is consistent with the integral argument of Gill [10] who showed that the transverse disturbances always decay for vertical isotropic layers; also see [11] for further analysis of this problem. Other roll orientations require numerical solution and, given the relatively straightforward nature of the stability problem as evidenced by Fig. 1 (i.e., that neutral curves are unimodal and that onset corresponds to stationary ($\mathrm{Im}(\lambda) = 0$) modes rather than to travelling ($\mathrm{Im}(\lambda) \neq 0$) modes) we may simply find the critical Rayleigh number in each case by imposing the condition $\partial R/\partial k = 0$. Therefore, we need to solve Eqs. (32) and (33) together with those formed by taking $\partial/\partial k$ of (32) and (33).

If we define $Q = \partial q/\partial k$ and $G = \partial g/\partial k$, then the full system we solve is

$$q'' - k^2(\xi_1 \sin^2\phi + \xi_3 \cos^2\phi)q - R\big[(\cos\alpha)g' + (\mathrm{i}k\xi_1 \sin\phi \sin\alpha)g\big] = 0, \tag{37}$$

$$g'' + \big[R\cos\alpha - k^2(\eta_1 \sin^2\phi + \eta_3 \cos^2\phi)\big]g - q' + (Rik\xi_1 \sin\phi \sin\alpha)\left(y - \frac{1}{2}\right)g - \mathrm{i}\lambda_I g = 0, \tag{38}$$

$$Q'' - k^2(\xi_1 \sin^2\phi + \xi_3 \cos^2\phi)Q - R\big[(\cos\alpha)G' + (\mathrm{i}k\xi_1 \sin\phi \sin\alpha)G\big] = 2k(\xi_1 \sin^2\phi + \xi_3 \cos^2\phi)q - (Ri\xi_1 \sin\phi \sin\alpha)g, \tag{39}$$

$$G'' + \big[R\cos\alpha - k^2(\eta_1 \sin^2\phi + \eta_3 \cos^2\phi)\big]G - Q' + (Rik\xi_1 \sin\phi \sin\alpha)\left(y - \frac{1}{2}\right)G - \mathrm{i}\lambda_I G = 2k(\eta_1 \sin^2\phi + \eta_3 \cos^2\phi)g - (Ri\xi_1 \sin\phi \sin\alpha) \times \left(y - \frac{1}{2}\right)g + \mathrm{i}\frac{\partial\lambda_I}{\partial k}g, \tag{40}$$

where λ_I is the imaginary part of λ (which was always computed to be zero), with $Re(\lambda) = 0$ defining neutrality. The appropriate boundary conditions are that

$$q' = g = Q' = G = 0 \quad \text{at} \quad y = 0, 1. \tag{41}$$

There are four eigenvalues to find, namely R, k, λ_I and $\partial\lambda_I/\partial k$ and therefore we require four normalisation conditions. Given that Eqs. (37)–(40) are complex, these four conditions are that

$$g'(0) = 1, \quad G'(0) = 0. \tag{42}$$

Eqs. (37)–(41) form a 16th-order system of real equations and they were solved by means of a variant of the Keller box method first introduced by Keller and Cebeci [12] in the context of boundary layer theory. Here we use a form suitable for ordinary differential eigenvalue problems and which was developed by Lewis et al. [13], although an independent study by Hsu and Wilks [14] uses a similar methodology. The equations are again approximated using second-order accurate central difference approximations whilst retaining second-order form in y, although the standard Keller box method reduces the equations to first-order form. The resulting system of algebraic equations are solved using a multi-dimensional Newton Raphson method. When properly

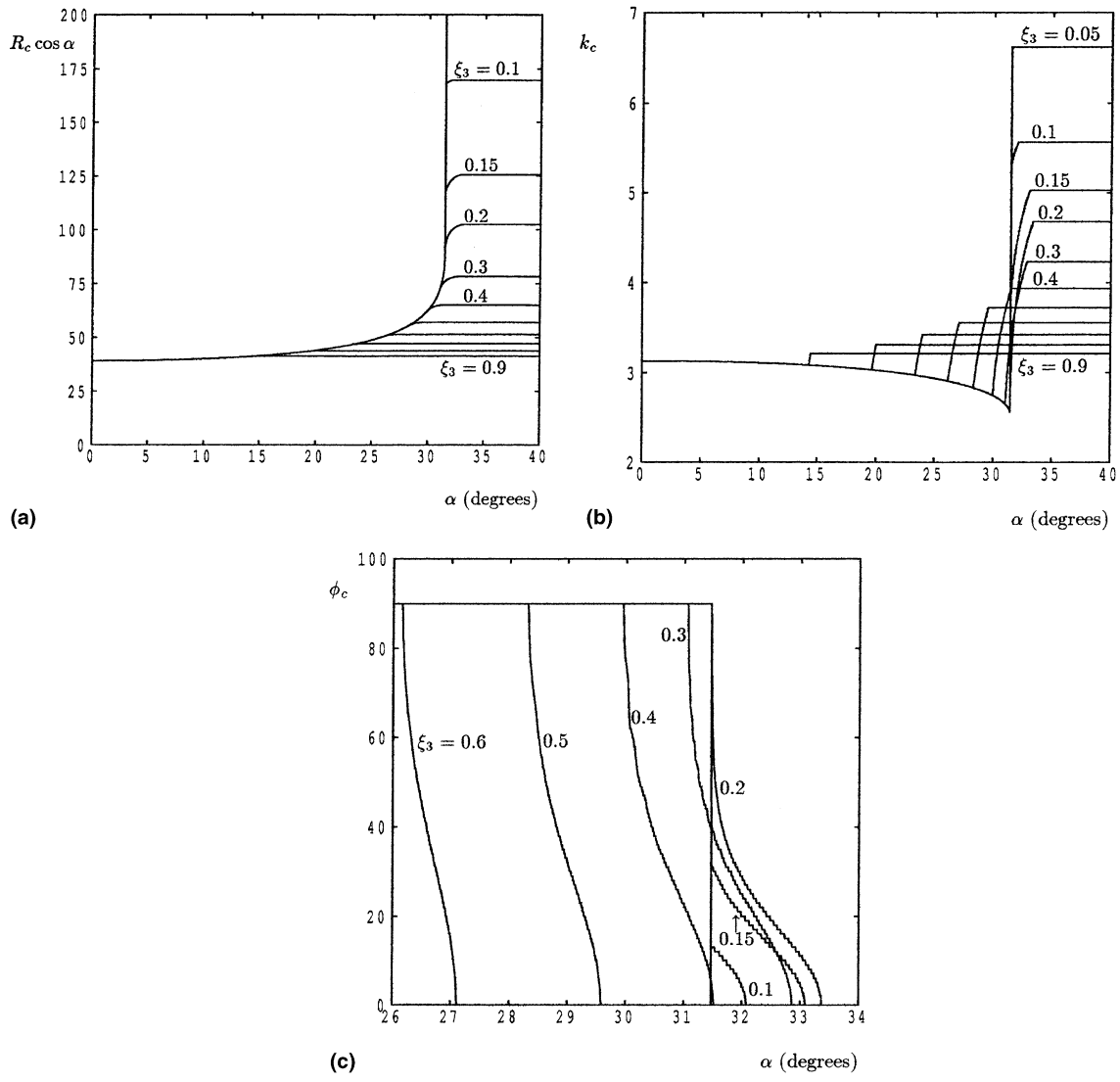

Fig. 6. Variation of (a) $R_c \cos\alpha$, (b) k_c and (c) ϕ_c with α. Minimisation of R_c over both k and ϕ has been imposed. Here we take $\xi_1 = \eta_1 = \eta_3 = 1$ for $\xi_3 = 0.05, 0.1, 0.15, 0.2, 0.3, \ldots, 0.9$.

ordered the iteration matrix takes a modified block tri-diagonal structure as illustrated below

$$\begin{pmatrix} B_1 & C_1 & & & & & E_1 \\ A_1 & B_2 & C_2 & & & & E_2 \\ & A_3 & B_3 & C_3 & & & E_3 \\ & & \ddots & \ddots & \ddots & & \vdots \\ & & & A_{N-1} & B_{N-1} & C_{N-1} & E_{N-1} \\ & & & & A_N & B_N & E_N \\ D_1 & D_2 & D_3 & \ldots & D_{N-1} & D_N & 0 \end{pmatrix} \begin{pmatrix} \underline{v}_1 \\ \underline{v}_2 \\ \underline{v}_3 \\ \vdots \\ \underline{v}_{N-1} \\ \underline{v}_N \\ \underline{l} \end{pmatrix} = \begin{pmatrix} \underline{r}_1 \\ \underline{r}_2 \\ \underline{r}_3 \\ \vdots \\ \underline{r}_{N-1} \\ \underline{r}_N \\ \mathcal{N} \end{pmatrix}. \tag{43}$$

Here $\underline{v}_i$ represents the error in the solution vector containing q, g, Q and G at the ith gridpoint; $\underline{l}$ is the error in the eigenvalues; $\underline{r}_i$ represents the finite difference approximation to the full Eqs. (37)–(40); A_i, B_i

and C_i are 8×8 matrices forming part of the Frechét derivative of $\underline{r}_i$ with respect to q, g, Q and G; $\mathcal{N}$ is composed of the four normalisation conditions supplemented by four dummy conditions in order to maintain eight rows in each block for convenience; D_i is the Frechét derivative of the normalisation condition; and E_i the Frechét derivative of $\underline{r}_i$ with respect to the eight eigenvalues (including the four dummy eigenvalues). All the entries in the matrix are computed using a straightforward numerical differentiation within the code, rather than being specified explicitly. Eq. (43) is solved by an extension of the block Thomas algorithm to account for the extra row and column as compared with the standard block tridiagonal structure.

On a practical note, this method, as expounded above, is of second-order accuracy and gives reasonably accurate results even when using a grid of 10 intervals. However, we found that much better accuracy was obtained by differentiating Eqs. (37) and (39) with respect to y and solving for q' and Q' rather than for q and Q. The difference in the absolute accuracy of the two approaches seems to lie with the fact that the former requires the satisfaction of derivative boundary conditions whereas the latter does not. In each run of the code the initial parameter set always corresponded to $\alpha = 0$ for which analytical solutions are available. For a chosen set of values of ξ_1, ξ_3, η_1 and η_3 the code followed the neutral curve using a straightforward curve-following methodology drawn from numerical bifurcation theory. In practice each new point on the curve was constrained to satisfy a proximity relation of the form

$$\left(\frac{\alpha_{n+1}-\alpha_n}{\mathrm{d}\alpha_{\max}}\right)^2 + \left(\frac{R_{n+1}-R_n}{\mathrm{d}R_{\max}}\right)^2 = 1, \tag{44}$$

where the subscript n denotes the number of steps taken along the neutral curve, and $\mathrm{d}\alpha_{\max}$ and $\mathrm{d}R_{\max}$ the maximum possible increments in α and R along the curve from point to point. This approach was deemed necessary because the neutral curves frequently have turning points, as depicted in Fig. 1 and which was also computed using this method.

We now present a comprehensive set of neutral curves for various values of ξ_3 , α and ϕ with $\eta_1 = \eta_3 = 1$. In Fig. 4(a)–(e) are shown the respective cases $\xi_3 = 3$, 1, 0.7, 0.15 and 0.05, where we show how the critical Rayleigh number varies with inclination for a set of roll orientations, ϕ. When $\xi_3 = 3$ (see Fig. 4(a)) longitudinal rolls form the preferred mode of instability for all inclinations of the layer. In fact this is true whenever $\xi_3 > 1$. When $\xi_1 = 1$ we recover the isotropic case displayed in Fig. 4(b). Here all modes have the same critical Rayleigh number when the layer is horizontal, but whenever the inclination is non-zero longitudinal modes are again preferred. Therefore, we concentrate on cases for which $\xi_3 < 1$ for the detailed results are more interesting. The variation of R_c with α is shown in Fig. 4(c) for $\xi_3 = 0.7$ and shows that when α is less than roughly 23.5° then transverse modes are dominant. It appears to be the case that there is then a sharp transition to longitudinal modes at higher inclinations. We will see later that this is not always true and that the transition may be smooth with the preferred orientation passing through all possible values from 90° to 0° over a short range of inclinations. That this truth may be seen in Fig. 5 where we show a close-up view of the transition point for the case $\xi_3 = 0.3$.

At smaller values of ξ_3 the local maximum (in terms of α) which is shown in Fig. 2 becomes crucially important. When ξ_3 is as low as 0.05, as shown in Fig. 4(e), then there is now an abrupt change in the preferred mode as α increases, and this arises because of that maximum. However, unlike the cases considered by Storesletten and Tveitereid [9], the sudden change in modes is also accompanied by a jump in the critical Rayleigh number and wave number. A transitional case is shown in Fig. 4(d), where $\xi_3 = 0.15$. There is again an abrupt change in the preferred mode from $\phi = 90°$, but now it is to a mode of non-zero orientation which then proceeds to vary smoothly towards zero as α increases.

These cases, and others are summarised in Fig. 6(a)–(c), where we show $\min_\phi R_c$ as a function of α together with the associated values of k_c and ϕ_c. All the observations derived from the subfigures of Fig. 4 may also be seen in these graphs. The critical orientation and the range of inclinations over which it changes smoothly are seen clearly in Fig. 5(c). The abrupt nature of the transition when ξ_3 is sufficiently small is also seen clearly in all three subfigures of Fig. 6. In Table 1 we indicate the

Table 1
Minimum and maximum values of α over which the transition from $\phi = 90°$ to $\phi = 0°$ takes place[a]

ξ_3	$\alpha_{\min}$	$\alpha_{\max}$	ϕ_{jump}
0.9	14.26	14.42	
0.8	19.63	20.00	
0.7	23.35	23.99	
0.6	26.15	27.11	
0.5	28.31	29.59	
0.4	29.94	31.52	
0.3	31.06	32.86	77
0.2	31.46	33.37	73
0.15	31.46	33.09	33
0.1	31.46	32.08	13
0.05	31.46	31.46	0

[a] When $\xi_3 > 0.35$ the transition is smooth. When $\xi_3 < 0.05$ the transition is sudden. In the intermediate range of values there is a sudden jump from $\phi = 90°$ to ϕ_{jump} followed by a smooth variation in ϕ towards 0°.

range of inclinations over which the smooth transition takes place.

The general pattern of behaviour for values of ξ_1 which are larger than unity is roughly the same as for when $\xi_1 = 1$. The general shape of the $\phi = 90°$ curve remains the same with a well-defined local maximum value of α at relatively small values of R and an asymptotic value of α when R is large. This means that the qualitative nature of the curves shown in Fig. 7, for which $\xi_3 = 3$, is the same as for those in Fig. 6. Now we find that longitudinal modes are always preferred when $\xi_3 > 3$. In fact, for thermally isotropic layers longitudinal modes are preferred whenever $\xi_3 > \xi_1$. The maximum value of α for transverse modes becomes larger as ξ_1 increases as does the critical Rayleigh number and wave number.

The corresponding curves for $\xi_1 = 0.3$ are shown in Fig. 8. For this value of ξ_3 the $\phi = 90°$ curve does not have a local maximum, and as shown in Fig. 2, the neutral curve has not yet attained an asymptotic value of the inclination. Therefore, we see a small qualitative difference between the respective curves shown in Figs. 7 and 8. For example, in Fig. 7(a) we see that the critical value of R for small values of ξ_3 increases gradually as α increases, but then changes discontinuously to a constant value at $\alpha \simeq 21°$. By contrast there appears not to be such a discontinuity in the corresponding curve in Fig. 8(a). The analysis of Rees and Bassom [7] evaluates the large-R behaviour of the neutral curve for the isotropic layer showing that it becomes vertical, and although a similar analysis is outside the scope of this paper, we assume that

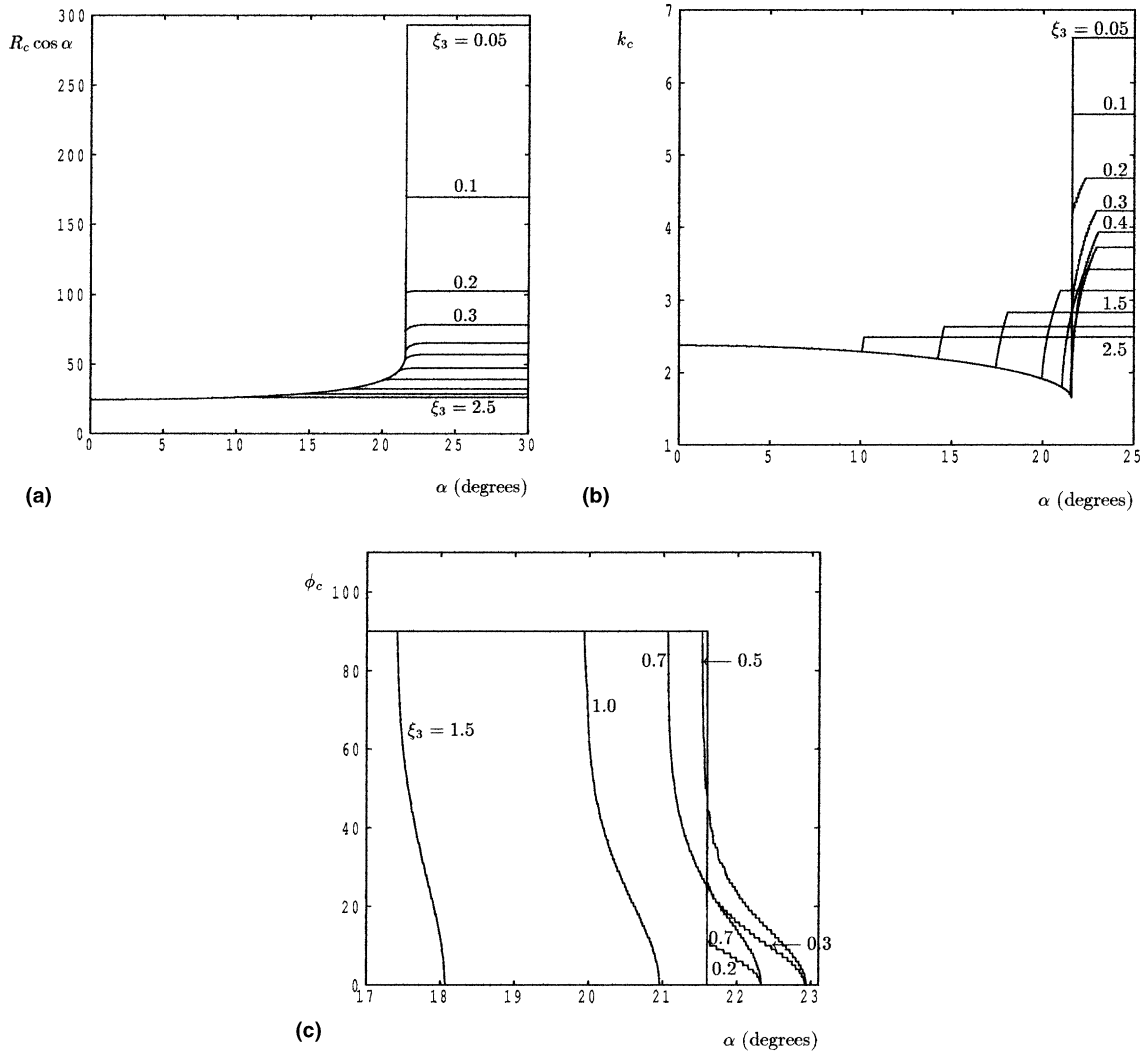

Fig. 7. Variation of (a) $R_c \cos\alpha$, (b) k_c and (c) ϕ_c with α. Minimisation of R_c over both k and ϕ has been imposed. Here we take $\xi_1 = 3$ and $\eta_1 = \eta_3 = 1$ for $\xi_3 = 0.05, 0.1, 0.15, 0.2, 0.3, 0.4, 0.5, 0.7, 1.0, 1.5, 2.0$ and 2.5.

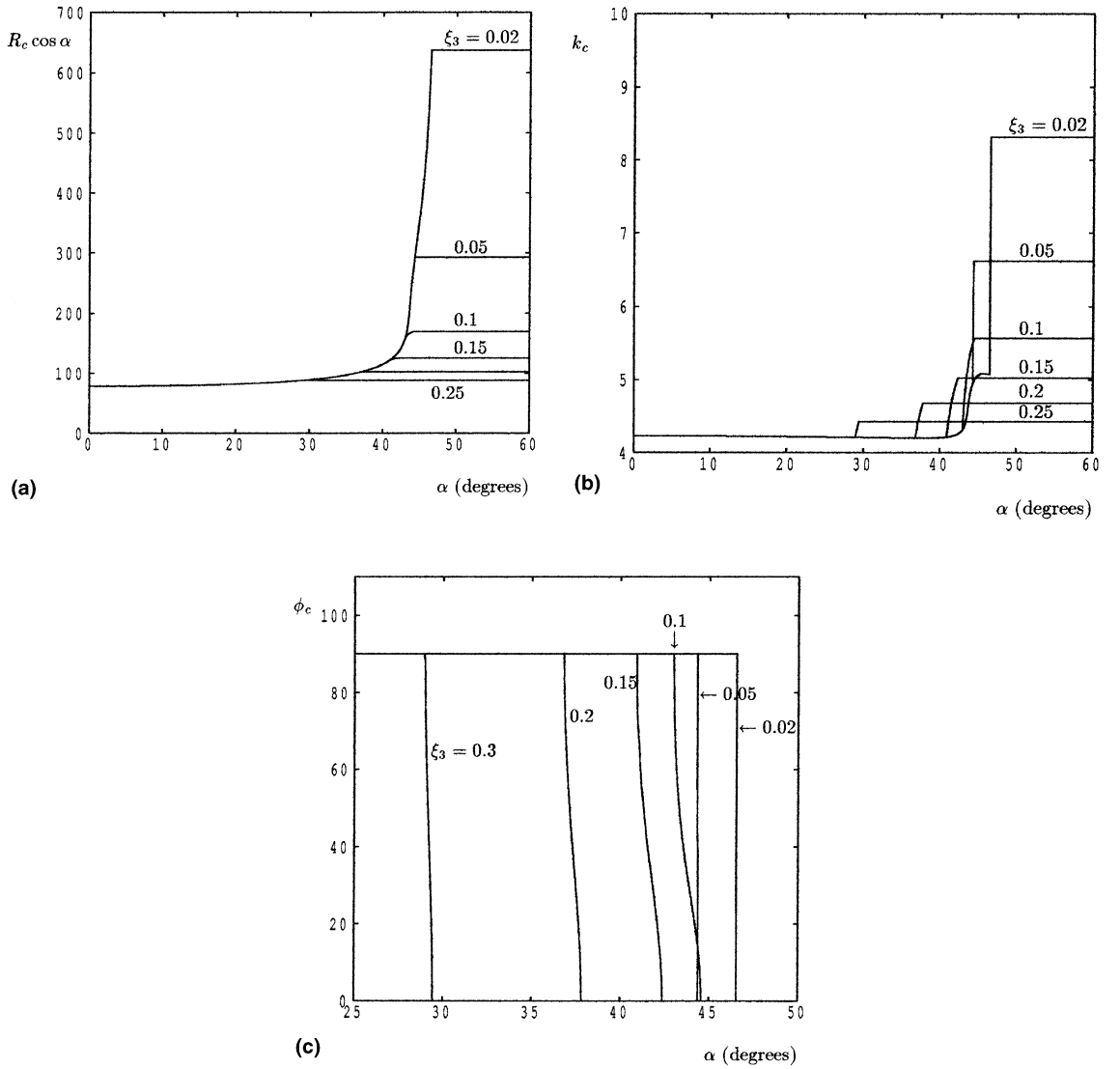

Fig. 8. Variation of (a) $R_c \cos\alpha$, (b) k_c and (c) ϕ_c with α. Minimisation of R_c over both k and ϕ has been imposed. Here we take $\xi_1 = 0.3$ and $\eta_1 = \eta_3 = 1$ for $\xi_3 = 0.02, 0.05, 0.1, 0.15, 0.2$ and 0.25.

such a similar behaviour exists for anisotropic media since the structure of the analysis should be identical.

5. Conclusions

In this study, we have made a detailed and extensive numerical analysis of the effects of anisotropy on the form of instability in an inclined porous layer heated from below. We have confirmed the results of Storesletten and Tveitereid [9] concerning circumstances when transverse rolls are to be favoured above longitudinal rolls. We have also extended the work contained in [9] to a wider parameter set. In general, either longitudinal rolls are favoured for all inclinations (such as when $\xi_3 > \xi_1$ in a thermally isotropic medium), otherwise there is a transition from transverse rolls at lower inclinations to longitudinal rolls at higher inclinations. However, we have found that this transition is not a straightforward exchange between transverse and longitudinal rolls, but rather the transition may be smooth (in terms of the angle of orientation of the favoured roll) or partly smooth and partly discontinuous when the anisotropy is more extreme. In the most extreme cases an immediate discontinuous transition between transverse and longitudinal modes

occurs. The critical wave numbers and Rayleigh numbers follow the same general behaviour as the critical orientation in terms of the degree of continuity of their dependence on the angle of inclination.

References

[1] C.W. Horton, F.T. Rogers, J. Appl. Phys. 16 (1945) 367–370.
[2] E.R. Lapwood, Proc. Camb. Philos. Soc. 44 (1948) 508–521.
[3] D.A.S. Rees, Stability of Darcy–Bénard convection, in: K. Vafai (Ed.), Handbook of Porous Media, Begell House, 2000, pp. 521–558.
[4] G. Castinel, M. Combarnous, C. R. Acad. Sci. Paris B 287 (1974) 701–704.
[5] L. Storesletten, Effects of anisotropy on convective flows through porous media, in: D.B. Ingham, I. Pop (Eds.), in: Transport Phenomena in Porous Media, Pergamon Press, Oxford, 1998, pp. 261–283.
[6] P. Vasseur, L. Robillard, Natural convection in enclosures filled with anisotropic porous material, in: D.B. Ingham, I. Pop (Eds.), Transport Phenomena in Porous Media, 1998, pp. 331–356.
[7] D.A.S. Rees, A.P. Bassom, The onset of Darcy–Bénard convection in an inclined layer heated from below, Acta Mech. 144 (2000) 103–118.
[8] A. Postelnicu, D.A.S. Rees, The onset of convection in an anisotropic porous layer inclined at a small angle from the horizontal, Int. Com. Heat Mass Trans., submitted for publication.
[9] L. Storesletten, M. Tveitereid, Appl. Mech. Eng. 4 (1999) 575–587.
[10] A.E. Gill, J. Fluid Mech. 35 (1969) 545–547.
[11] S. Lewis, A.P. Bassom, D.A.S. Rees, Eur. J. Mech. B: Fluids 14 (1995) 395–408.
[12] H.B. Keller, T. Cebeci, Accurate numerical methods for boundary layer flows 1. Two dimensional flows, in: Proceedings of the International Conference on Numerical Methods in Fluid Dynamics, Lecture notes in Physics, Springer, New York, 1971.
[13] S. Lewis, D.A.S. Rees, A.P. Bassom, Q. J Mech. Appl. Math. 50 (1997) 545–563.
[14] J.J. Hsu, G. Wilks, J. Fluid Mech. 300 (1995) 207–229.